Real-time Imaging and Holdup Measurement of Carbon Dioxide under CCS Conditions Using Electrical Capacitance Tomography

Shijie Sun, *Member, IEEE*, Wenbiao Zhang, *Member, IEEE*, Jiangtao Sun, *Member, IEEE*, Zhang Cao, *Member, IEEE*, Lijun Xu*, *Senior Member, IEEE*, Yong Yan, *Fellow, IEEE*

***Abstract*- This paper presented a method for real-time cross-sectional imaging and holdup measurement of gas-liquid two-phase carbon dioxide (CO_2) flow using electrical capacitance tomography (ECT). A high-pressure ECT sensor with 12 electrodes was constructed and a dedicated digital ECT system with a data acquisition rate of 757 frames per second was developed for capacitance measurement. Three widely-used image reconstruction algorithms were compared for tomographic imaging and phase holdup measurement. Experiments were carried out on a DN25 laboratorial scale CO_2 two-phase flow rig at a pressure of 6 MPa for the gaseous mass flowrates from 0 to 430 kg/h and liquid mass flowrates at 515, 1100 and 1900 kg/h. The experimental results show that the cross-sectional distribution of two-phase CO_2 flow can be monitored using the ECT system, which matches well with the images captured by a high-speed imaging system. Compared with the reference gas holdup obtained by the flowmeters in the single phase gaseous and liquid loops, the absolute accuracy of the gas holdup measurement can reach 6%, indicating that the developed system is promising for real-time monitoring of carbon dioxide in CCS transportation pipelines.**

***Keywords*- Electrical capacitance tomography, Carbon dioxide transport, Image reconstruction, Holdup measurement**

I. Introduction

Carbon dioxide (CO_2) is the most significant long-lived greenhouse gas in the atmosphere [1]. Since the industrial revolution, a large amount of CO_2 has been produced due to the burning of coal, oil and gas. The increasing emission of CO_2 has leading to serious problems, such as global warming and ocean acidification. Carbon Capture and Storage (CCS) technique is a potential means to prevent the release of large quantities of CO_2 into the atmosphere, which has attracted worldwide attentions [2].

This work was supported by the National Natural Science Foundation of China (No. 61620106004 and 61522102) and National Postdoctoral Program for Innovative Talents (No. BX201700021).

S. Sun, L. Xu, J. Sun and Z. Cao are with Beijing Advanced Innovation Center for Big Data-Based Precision Medicine, Beijing, China and the Key Laboratory of Precision Opto-Mechatronic Technology of Ministry of Education, the School of Instrument Science and Opto-Electronic Engineering, Beihang University, Beijing, 100191, China (e-mail: lijunxu@buaa.edu.cn)

W. Zhang is with School of Control and Computer Engineering, North China Electric Power University, Beijing, 102206, China.

Y. Yan is with School of Engineering and Digital Arts, University of Kent, Canterbury, CT2 7NT, UK

CCS is the process of capturing CO_2 from large point sources, such as fossil fuel power plants, transporting it to a suitable storage site, and depositing it where it will not enter the atmosphere, normally an underground geological formation [3], [4]. This paper focuses on the carbon dioxide transport process, most likely through pipelines because of the cheapest cost.

Monitoring and holdup measurement of the CO_2 flow are essential to monitor and accurately account the captured CO_2 across the CCS chain and help prevent leakage during transport [5]. During the pipeline transport, CO_2 is maintained as dense liquid phase under high pressure (>5Mpa) to increase the transport efficiency. Due to thermodynamic properties of CO_2, minor variations in temperature and pressure will result in phase change of CO_2 and the CO_2 flow will become a gas-liquid two-phase flow. In this case, it is challenging to monitor the flow condition and provide accurate measurements using traditional flowmeters.

In the literatures, the Orifice flowmeter has been used for the measurement of slugging gas-liquid flow, but the error can reach up to 80% [6]. The Coriolis mass flowmeter can also be applied to measure gas-liquid CO_2 flow [6], [7]. However, the techniques based on these flowmeters cannot provide distribution information of the two phases.

In the last decades, several tomographic techniques have been developed to monitor two-phase flows including ultrasonic [8] and electrical methods [9], [10]. Each technique makes use of differences between physical characteristics of the two phases and is suitable for specific applications [11]. For example, the electrical impedance tomography technique has been applied to monitor solid-liquid and gas-liquid flows [12].

Among these tomographic techniques, electrical capacitance tomography (ECT) is an imaging technique to obtain the permittivity distribution in the interior of the pipe from capacitance measurements at external boundary [13]–[15]. ECT is one of the most promising techniques for multi-phase flow measurement, which has been successfully applied to gas-oil two-phase flows in oil industry [16] and gas-liquid-solid three-phase flows [17]. It has several advantages such as low cost, high speed and non-invasive compared with other tomographic techniques [15], [18], [19].

In this paper, the ECT technique is introduced to flow

process monitoring and holdup measurement of CO_2 two-phase flow because of the following two reasons: 1) Compared with sensors of other electrical tomography modalities, such as electrical resistance tomography (ERT) [20], ECT sensors are not required to directly contact with the high-pressure CO_2 fluid. Compared with optical and ultrasonic sensors, ECT sensors have simpler configuration [21]; 2) The permittivities of gaseous CO_2 and liquid CO_2 are 1 and 1.6, respectively, which are both non-conducting. In this application scenario, ECT can be applied while ERT cannot.

However, it is still a challenging task to accurately account and monitor the CO_2 flow using ECT. Firstly, the structure of the ECT sensor should be carefully designed for high-pressure conditions to prevent CO_2 leakage. Secondly, the permittivities of gas CO_2 and liquid CO_2 are close to each other and the two phases change rapidly, which requires an accurate and fast capacitance measurement system and an anti-noise image reconstruction algorithm.

In this research, a high-pressure ECT sensor was constructed and a high-performance digital ECT system was developed. Three typical algorithms were evaluated regarding image reconstruction and holdup calculation. Experiments were performed on a two-phase CO_2 flow rig to verify the feasibility of the proposed technique.

II. Design of the ECT System

A. High-pressure ECT sensor

The ECT technique is used to obtain the permittivity distribution of the two-phase CO_2 flow inside the conveying pipeline. A typical ECT sensor consists of a number of electrodes, which are placed around the periphery of the pipeline.

A high-pressure ECT sensor is designed in this paper, which can withstand the pressure of 10 MPa. The cross-sectional view of the sensor is shown in Fig. 1. The ECT sensor consists of 12 brass electrodes of 40 mm in length, which are symmetrically placed around the periphery of a polytef pipe. The inner diameter of the pipe is 25 mm, while the outer diameter is 31 mm. A piece of brass foil is wrapped around the electrodes for shielding.

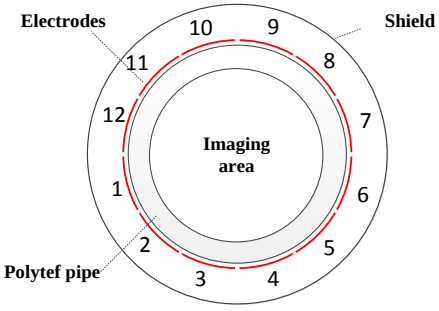

Fig. 1. Cross-sectional view of the ECT sensor.

To withstand the high pressure inside the pipe, a stainless steel pipe section is placed outside the polytef pipe. Sufficient epoxy resin and curing agent are injected into the space between the two pipe sections. When the epoxy resin is completely cured, the two pipes are fixed tightly with bolts and nuts. The design sketch of the ECT sensor is shown in Fig. 2. The spool piece is installed on the pipeline using flanges.

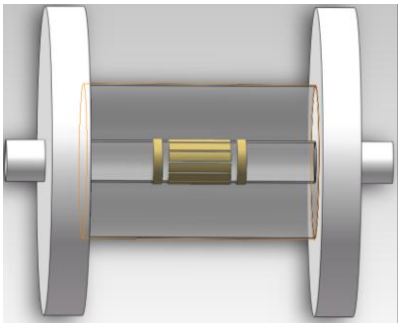

Fig. 2. Design sketch of the ECT sensor.

B. Capacitance measurement unit

A capacitance measurement unit is developed to measure the capacitances between every two electrodes of the ECT sensor, including one capacitance measurement circuit and several multiple CMOS switches. The schematic configuration is shown in Fig. 3.

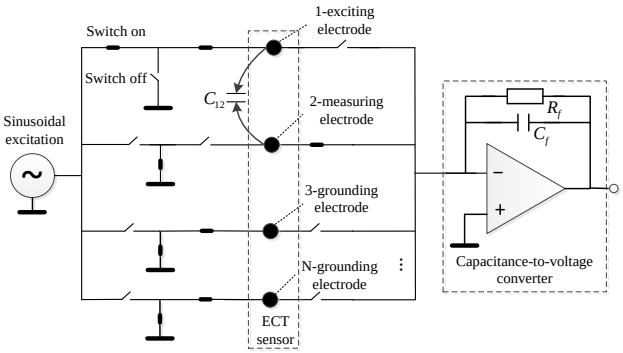

Fig. 3. Schematic diagram of the capacitance measurement unit.

The capacitance measurement circuit consists of a Complex Programmable Logic Device (CPLD), a Digital-to-Analog Converter (DAC), an Analog-to-Digital Converter (ADC), a capacitance-to-voltage (C-V) converter, a Low-pass filter (LPF) and an internet interface device. The CPLD is used for channel selection, signal demodulation and logic control. A sine-wave excitation signal is generated by CPLD, DAC, and LPF based on the Direct Digital Synthesize (DDS) technique. The capacitance is measured with the C-V converter using AC-based method [15], [19]. The internet device is used for data communication between the capacitance measurement unit and the host PC.

The excitation frequency is 100 kHz and the duration of each capacitance measurement is 10 μs. By using the CMOS switches, the capacitance between every two electrodes can be measured one after another. A time interval of 10 μs is

added between two adjacent measurements to reduce the influences of switching oscillations. The data acquisition rate of the proposed measurement unit is 757 frames per second.

III. Image Reconstruction and Holdup Calculation

A. Image reconstruction

The permittivity distribution can be reconstructed by measuring the capacitance values between every two electrodes and using a suitable reconstruction algorithm. A number of reconstruction algorithms have been developed in recent years, which can be divided into two types, i.e., non-iterative algorithm and iterative algorithm. In this paper, three widely-used algorithms are introduced and used for image reconstruction.

1) Linear back projection (LBP) algorithm

In the LBP algorithm, the relationship between the measured capacitances and permittivity distribution is simplified to a linear form [22].

$$\Delta C = J\Delta\varepsilon, \tag{1}$$

where ΔC is the capacitance change, Δε is the permittivity change and J is the sensitivity matrix of the capacitance versus permittivity distribution. In general, equation (1) is written in a normalized form

$$\lambda = Sg, \tag{2}$$

where λ is the normalized capacitance vector, S is the sensitivity matrix of normalized capacitance with respect to normalized permittivity vector, and g is the normalized permittivity vector, i.e. the pixel values to be imaged. An approximated solution of g is given as

$$g_{LBP} = (S^T\lambda)./(S^T f_\lambda), \tag{3}$$

where f_λ=[1,1,⋯,1] and g_{LBP} is the reconstructed permittivity vector. The LBP algorithm is simple and suitable for online image reconstruction. However, it provides poor-quality images.

2) Landweber algorithm

Iterative algorithms are developed to improve the reconstructed image quality. The projected Landweber algorithm is the most widely used iterative algorithm [23], [24].

$$g_{k+1} = P[g_k - \alpha S^T(Sg_k - \lambda)], \tag{4}$$

where α is a relaxation factor, P is a projection operator and

$$P[f(x)] = \begin{cases} 0 & f(x) < 0 \\ f(x) & 0 \le f(x) < 1 \\ 1 & f(x) > 1 \end{cases}, \tag{5}$$

The main drawbacks of the iterative algorithm are that it is time-consuming and a suitable relaxation factor and stop criteria for the iterations need to be pre-determined.

3) Calderon algorithm

Unlike the sensitivity-matrix-based algorithms described above, the Calderon algorithm can independently provide the gray value at any pixel of the reconstructed image using a direct approach. The Calderon algorithm is time-saving as no matrix inversion or iterative process is involved and it is suitable for imaging of low contrast dielectrics [25].

For ECT, the governing equation of the sensing field, denoted by Ω, is

$$\nabla\cdot\varepsilon(z)\nabla\varphi(z) = 0, \tag{6}$$

where $z=x+iy$ represents the point with coordinates (x, y), $\varepsilon(z)$ and $\varphi(z)$ are the permittivity and electrical potential at z.

According to the divergence theorem, the relationship between the integrals of the spatially varying permittivity and voltage and current measurements on the boundary is

$$\int_\Omega \upsilon(z)\nabla\varepsilon(z)\nabla\varphi(z)dz = \int_{\partial\Omega}\upsilon(z)\varepsilon(z)\frac{\partial\varphi(z)}{\partial n}dl - \int_\Omega \nabla\upsilon(z)\varepsilon(z)\nabla\varphi(z)dz = 0, \tag{7}$$

where $\upsilon(z)$ is an arbitrary continuous function in L2-space and dl is the measured arc length on the boundary $\partial\Omega$.

Denote the voltage-to-current density map, i.e., the Dirichlet-Neumann map, as

$$\Lambda_\varepsilon : \varphi(z)|_{\partial\Omega} \to \varepsilon(z)\frac{\partial\varphi(z)}{\partial n}|_{\partial\Omega}, \tag{8}$$

where Λ_ε denotes the voltage-to-current density map when Ω contains $\varepsilon(z)$. Equation (7) can be rewritten as

$$\int_\Omega \varepsilon(z)\nabla\upsilon(z)\nabla\varphi(z)dz = \int_{\partial\Omega}\upsilon(z)\Lambda_\varepsilon(\varphi(z))dl, \tag{9}$$

For a disturbed permittivity $\varepsilon(z)=1+\delta\varepsilon(z)$ and if this change only exists in Ω, we obtain

$$\begin{aligned}\delta\varepsilon(x,y) &= \delta\varepsilon(z) \\ &\approx \frac{1}{2\pi^2}\iint_{R^2}\frac{t(k_1+ik_2)}{k_1^2+k_2^2}e^{i(-2k_1,2k_2)\cdot(x,y)}dk_1dk_2\end{aligned}, \tag{10}$$

and the scattering transform t(k) is

$$t(k) \approx -2(k_1^2+k_2^2)\iint_\Omega \delta\varepsilon e^{-i(-2k_1,2k_2)\cdot(x,y)}dxdy, \tag{11}$$

where $k=k_1+ik_2$. Then the disturbed permittivity can be obtained from (10). In the polar coordinates of parameters r and θ, equation (10) can be rewritten as

$$\delta\varepsilon(x,y) \approx \frac{1}{2\pi^2}\int_0^{R_0}\int_{-\pi}^{\pi}\frac{t(re^{i\theta})}{r}e^{i2r(-\cos\theta,\sin\theta)\cdot(x,y)}d\theta dr, \tag{12}$$

where R_0 is the radius of the region used for the numerical integration.

B. Holdup calculation

Based on the above-mentioned ECT hardware and image reconstruction algorithms, the flow pattern of the two-phase CO_2 flow can be identified and the gas holdup can be calculated.

Firstly, the capacitances between every two electrodes when the pipe is full of gaseous CO_2 or liquid phase CO_2 are measured for calibration.

Secondly, the permittivity distribution ε is reconstructed using an image reconstruction algorithm. The normalized permittivity distribution is calculated by

$$\varepsilon_m^{Norm} = \frac{\varepsilon_m - \varepsilon_{low}}{\varepsilon_{high} - \varepsilon_{low}}, \tag{13}$$

where ε_m, ε_{low} and ε_{high} are the reconstructed permittivity distribution of the CO_2 flow, gaseous CO_2 and liquid phase

CO_2.

Thirdly, a series of ECT images of normalized permittivity distribution is obtained within a short time period to identify the flow pattern.

Finally, the gas holdup can be calculated by

$$h = 1 - \frac{\sum_{i=1}^{L} \varepsilon_m^{Norm}(i)}{L}, \tag{14}$$

where L is the number of pixels in the reconstructed image and $\varepsilon_m^{Norm}(i)$ is the i-th pixel of normalized permittivity value. In this paper, as the sensor electrodes are rectangle and 40 mm long, the cross-sectional images reconstructed by ECT represent the averaged permittivity distribution within the axial coverage of the electrodes. In the cross-sectional area, the flow velocity profile is not uniform. If we want to obtain a more accurate volume holdup, the velocity information should be considered. However, the velocity information cannot be obtained using the present structure of ECT sensor, which needs to be further studied.

IV. Experimental Results

A. Experimental setup

The schematic diagram and photo of the DN25 experimental setup are shown in Fig. 4 and Fig. 5, including three main pipelines for gaseous phase, liquid phase and gas-liquid two-phase CO_2 flow. Coriolis mass flowmeters are installed in gas and liquid phase loops to obtain the mass flow rates, temperatures and densities of the gas and liquid single-phase flows, respectively. A sight window and the ECT sensor were mounted next to the mixer. A high speed imaging system was used to capture the image of the CO_2 flow through the sight window.

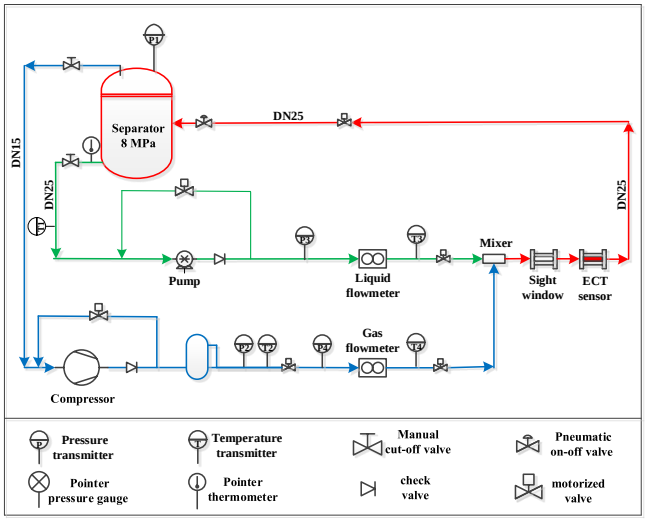

Fig. 4. Schematic diagram of experimental setup.

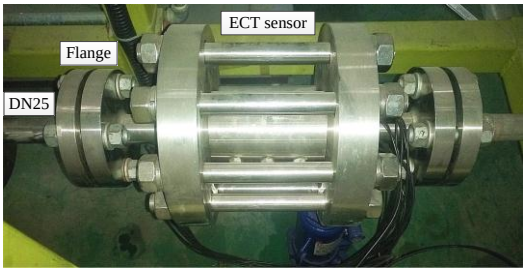

Fig. 5. Photo of experimental setup.

B. Experiment

The experiment was performed under laboratorial conditions at 22 ℃ and 101 kPa ambient. In the experiment, by setting the liquid CO_2 flowrates at 515, 1100 and 1900 kg/h and increasing the gaseous CO_2 flowrate stepwise from 0 to 430 kg/h, the gas-liquid two-phase CO_2 flow with different gas holdups can be generated through a mixer. The sight window and the ECT sensor are mounted next to the mixer and the pressure in the pipelines is 6 Mpa and kept stable. Therefore, the phase change of the CO_2 flow is small between the sight window and the ECT sensor.

The reference gas holdup is calculated using the measured flow rates, temperatures and densities of the two single-phase flows. Assume that m_g and m_l be the mass flowrates of the gaseous and liquid CO_2 flow, ρ_g and ρ_l be the densities of the gaseous and liquid CO_2 flows, respectively. Then superficial gas velocity and superficial liquid velocity of the CO_2 flow can be calculated by

$$\begin{cases} u_g = \dfrac{m_g}{\rho_g \pi r^2}, \\ u_l = \dfrac{m_l}{\rho_l \pi r^2} \end{cases} \tag{15}$$

The reference gas holdup of the gas-liquid two-phase CO_2 flow is

$$h_g = \frac{m_g / \rho_g}{m_g / \rho_g + m_l / \rho_l}, \tag{16}$$

C. Results

1) Liquid flowrate at 515 kg/h

Firstly, the liquid flowrate is set to be 515 kg/h and the gas flowrate ranges from 0 to 430 kg/h, resulting in a reference gas holdup ranging from 0 to 77%. When the gas-liquid two-phase CO_2 flow becomes stable, images were captured by the high-speed imaging system, as shown in Fig. 6.

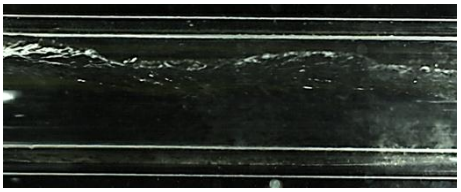

(a) reference gas holdup-20%

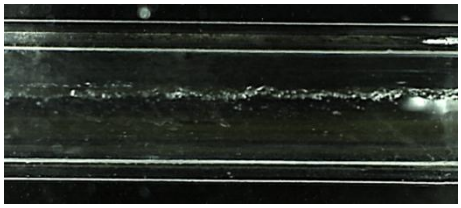

(b) reference gas holdup-40%

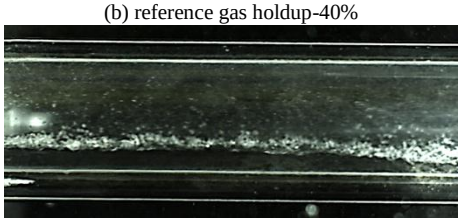

(c) reference gas holdup-60%

Fig. 6. Images captured by the high-speed imaging system for different gas holdups when the liquid flowrate is 515 kg/h.

The images reconstructed by the ECT system are shown in Fig. 7. For the Landweber algorithm, it is crucial to select a suitable relaxation factor and number of iterations, which greatly affect the reconstruction result. According to Tian *et al.* [24], the relaxation factor is chosen to be 0.5 and the number of iterations is 8. For the Calderon method, the radius of the region used for the numerical integration is set to be 1.8. In the ECT images, the blue and red colors represent low and high permittivities, respectively. The blue outer ring in each image reperesents the wall of the polytef pipe. For the ECT images from left to right, the corresponding gas holdup changes from 0 to 77%. The last image at each row is reconstructed when the ECT sensor is filled with gaseous CO_2.

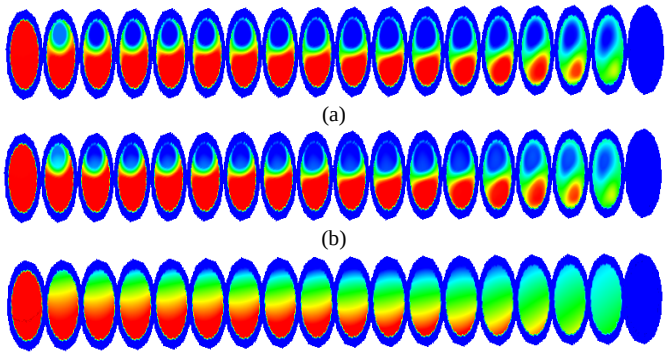

(a)

(b)

(c)

Fig. 7. Variation of cross-sectional images reconstructed by ECT with gas holdup obtained by using (a) LBP algorithm, (b) Landweber algorithm and (c) Calderon algorithm when the liquid flowrate is 515 kg/h.

From Fig. 6 and Fig. 7, it can be seen that the gaseous CO_2 and liquid CO_2 can be distinguished via ECT imaging of permittivity distributions. The flow pattern of the CO_2 flow at lower liquid flowrate is obviously stratified flow, which can be recognized via image reconstruction using the three algorithms. The boundary between the gaseous CO_2 and liquid CO_2 obtained using the LBP and Landweber algorithms is more obvious than that using the Calderon algorithm. When the gas flowrate increases, the gas holdup increases and the area of blue region increases in the ECT images.

The reconstructed permittivity distributions are then used to calculate the gas holdup. To evaluate the measurement accuracy, the absolute error is defined as

$$e_a = h_m - h_r , \tag{17}$$

where h_m is the gas holdup measured by ECT and h_r is the reference gas holdup. The standard deviation is defined as

$$\sigma = \sqrt{\frac{\sum_{i=1}^{M}\left[h(i)-\bar{h}\right]^2}{M-1}} , \tag{18}$$

where $h(i)$ is the i-th gas holdup value measured by ECT, and $\bar{h}$ and M are the average gas holdup value and the total number of measurements by ECT, respectively.

The absolute errors and standard deviations of the gas holdup measurement by ECT at lower liquid flowrate are shown in Fig. 8. The upper triangular blocks, square blocks and plus signs represent the gas holdups calculated using the LBP, Landweber and Calderon algorithms, respectively.

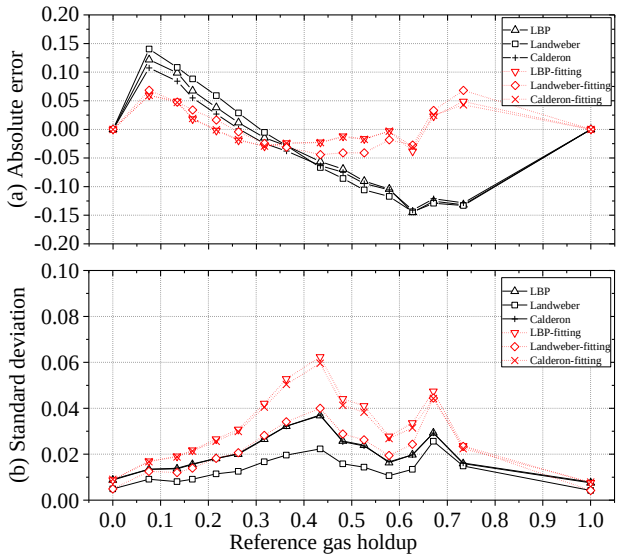

Fig. 8. (a) Absolute errors and (b) standard deviations of gas holdup measurements by ECT when liquid flowrate is 515 kg/h.

In general, we expect that the relationship between the measured gas holdup and reference gas holdup is linear. However, the relationship is determined by a polynomial. Here, a third order polynomial is used to fit the curve. Then the fitted gas holdup curve can be described by

$$h_c = p_1 h_m^3 + p_2 h_m^2 + p_3 h_m + p_4 , \tag{19}$$

The coefficients of the polynomial are calculated using the least squares method. Then the calculated p_1, p_2, p_3 and p_4 are -2.66, 3.46, 0.22 and -0.02 for the LBP algorithm, -3.11, 4.07, 0.06 and -0.03 for the Landweber algorithm, and -2.25, 2.84, 0.44 and -0.03 for the Calderon algorithm, respectively.

In Fig. 8, the lower triangular blocks, diamond blocks and multiple signs represent the fitted gas holdups for the LBP, Landweber and Calderon algorithms, respectively. As seen from the fitted results, the maximum absolute errors are 6.0%,

6.8% and 6.0%, and the maximum standard deviations are 6.2%, 4.4% and 6.0% for the LBP, Landweber and Calderon algorithms, respectively. Overall, the three algorithms provide similar absolute errors. The Landweber algorithm provides lower standard deviation because the iteration process acts as a filter and reduces the noises. The standard deviation can be reduced by averaging more measurements at an expense of measurement speed.

In Fig. 6, it is shown that at a lower liquid flowrate, the flow pattern is stratified flow and the boundary between the two-phases fluctuates sharply, leading to a wavy flow and a larger measurement uncertainty. In Fig. 8 (b), when the gas holdup becomes close to 50%, the boundary area of the two phases becomes larger, resulting in a larger standard deviation and measurement uncertainty. Compared with a calm stratified flow, more measurements are required for averaging to reduce the measurement uncertainty in this case.

2) Liquid flowrate at 1100 kg/h

The medium liquid flowrate is set to be 1100 kg/h and the gas flowrate ranges from 0 to 430 kg/h, resulting in a reference gas holdup ranging from 0 to 60%. The images of the CO_2 flow captured by the camera and reconstructed by ECT are shown in Fig. 9 and Fig. 10, respectively. For the Landweber algorithm, the relaxation factor is chosen to be 0.5 and the number of iterations is 70. For the Calderon method, the radius of the region used for the numerical integration is set to be 1.8.

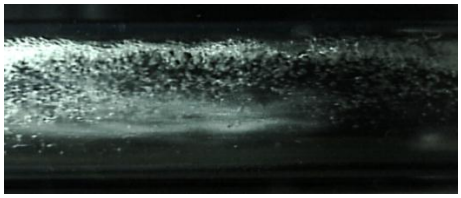

(a) reference gas holdup-12%

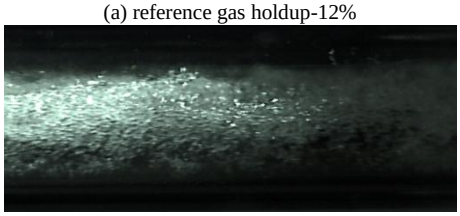

(b) reference gas holdup-21%

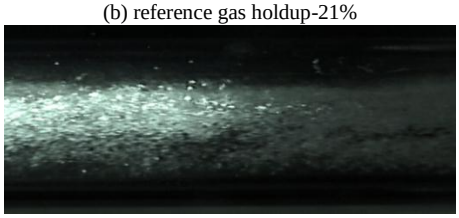

(c) reference gas holdup-39%

Fig. 9. Images captured by the high-speed imaging system for different gas holdups when the liquid flowrate is 1100 kg/h.

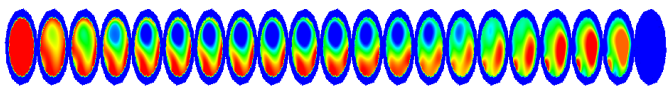

(a)

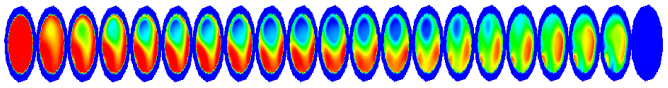

(b)

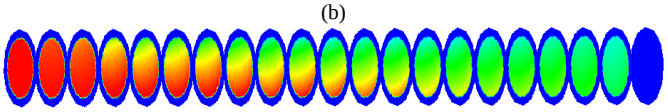

(c)

Fig. 10. Variation of cross-sectional images reconstructed by ECT with gas holdup obtained by using (a) LBP algorithm, (b) Landweber algorithm and (c) Calderon algorithm when the liquid flowrate is 1100 kg/h.

When the liquid flowrate is 1100 kg/h, the flow pattern of the CO_2 flow is bubble flow. The gas holdup in the upper area is larger than that in the lower area. The ECT images show the rising tendency of the gas holdup.

The absolute errors of the gas holdups measured by ECT and corresponding standard deviations are shown in Fig. 11. After fitted using the least squares method, the maximum absolute errors are 3.9%, 5.2% and 3.2%, and the maximum standard deviations are 5.9%, 3.5% and 5.1% for the LBP, Landweber and Calderon algorithms, respectively.

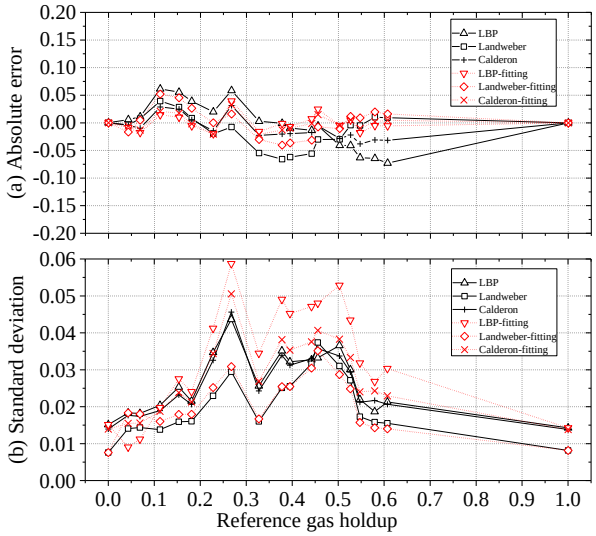

Fig. 11. (a) Absolute errors and (b) standard deviations of gas holdups measured by ECT when liquid flowrate is 1100 kg/h.

3) Liquid flowrate at 1900 kg/h

The high liquid flowrate is set to be 1900 kg/h and the gas flowrate ranges from 0 to 430 kg/h, resulting in a reference gas holdup ranging from 0 to 40%. The images of the CO_2 flow captured by the camera and reconstructed by ECT are shown in Fig. 12 and Fig. 13, respectively. For the Landweber algorithm, the relaxation factor is chosen to be 1 and the number of iterations is 100. For the Calderon method, the radius of the region used for the numerical integration is set to be 1.8.

In Fig. 12, it is shown that the gaseous CO_2 and liquid CO_2 are evenly mixed when the liquid flowrate is 1900 kg/h. From Fig. 13, the images reconstructed using the Calderon algorithm agree well with the camera images. The small bubbles cannot be distinguished due to the low resolution of the ECT images. The images reconstructed using the LBP and

Landweber algorithms show some inhomogeneity of the two-phase flow but are of distortion.

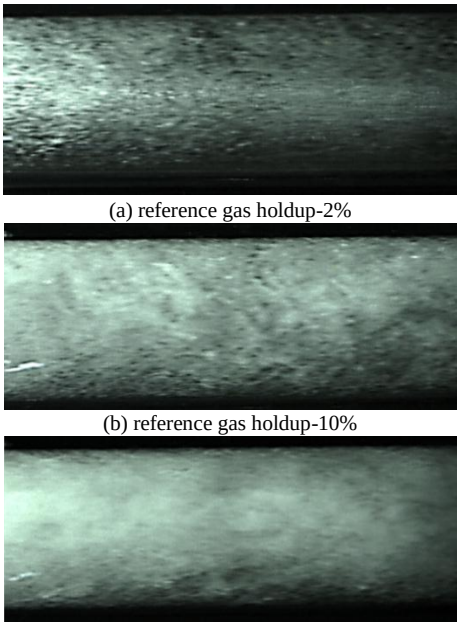

(a) reference gas holdup-2%

(b) reference gas holdup-10%

(c) reference gas holdup-24%

Fig. 12. Images captured by the high-speed imaging system for different gas holdups when the liquid flowrate is 1900 kg/h.

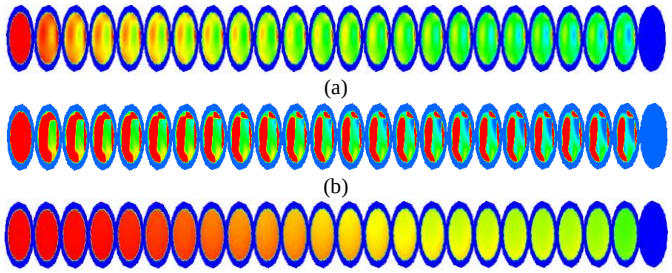

(a)

(b)

(c)

Fig. 13. Variation of cross-sectional images reconstructed by ECT with gas holdup obtained by using (a) LBP algorithm, (b) Landweber algorithm and (c) Calderon algorithm when the liquid flowrate is 1900 kg/h.

The absolute errors of the gas holdups measured by ECT and corresponding standard deviations are shown in Fig. 14. After fitted, the maximum absolute errors are 1.3%, 1.3% and 1.6%, and the maximum standard deviations are 3.1%, 2.5% and 3.1% for the LBP, Landweber and Calderon algorithms, respectively.

When the gaseous CO_2 and liquid CO_2 are evenly mixed, the two-phase flow becomes symmetrical in geometry. Compared with the results at lower liquid flowrate, the standard deviation becomes lower and hence a lower measurement uncertainty can be obtained.

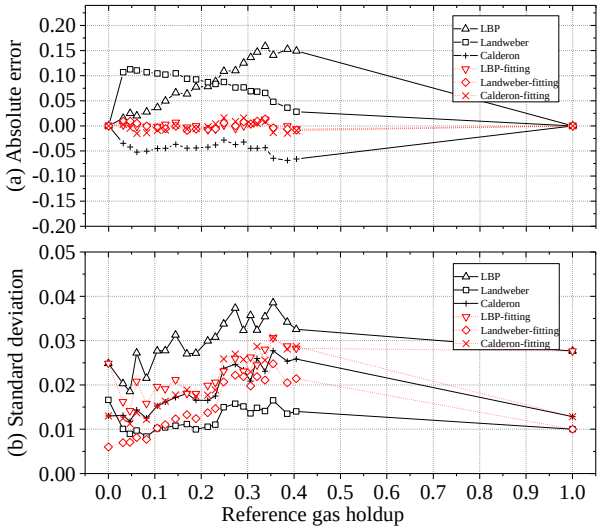

Fig. 14. (a) Absolute errors and (b) standard deviations of the gas holdups measured by ECT when liquid flowrate is 1900 kg/h.

4) Dynamic process monitoring

A dynamic process of the two-phase CO_2 flow was monitored by the proposed ECT system. The pipe was firstly filled with gaseous CO_2. Then the pump in the liquid phase loop was started and liquid phase CO_2 was ejected into the pipe until all the pipe was filled with liquid phase CO_2. The variation in the liquid holdup against the measurement time was shown in Fig. 15.

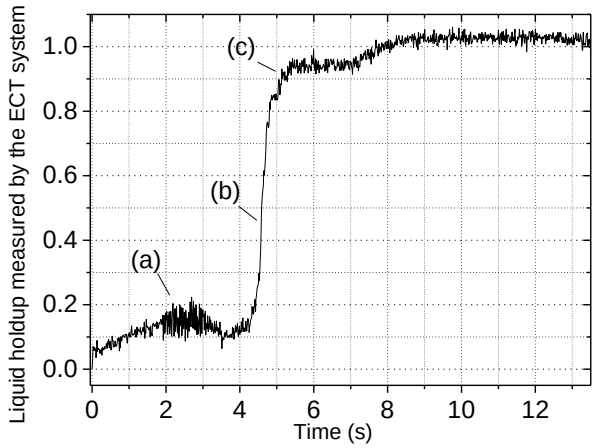

Fig. 15. Variation in liquid holdup against measurement time.

Totally, 757 measurements of liquid holdup can be obtained using ECT and the dynamic process can be clearly reflected from those results. The images captured by the camera at the three typical time points of (a), (b) and (c) in Fig. 15 are shown in Fig. 16.

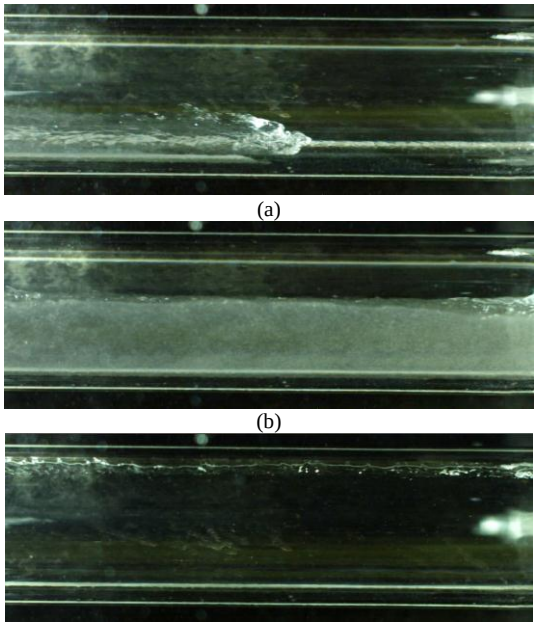

(a) (b) (c)

Fig. 16. Images captured by camera at time points of (a), (b) and (c).

From Fig. 16, the flow pattern in the dynamic process is liquid slug-stratified-bubbly flow. The liquid holdup measured by ECT changes with the increasing transferred liquid CO_2. The liquid holdup dramatically increases in the period from 4 to 5 second in Fig. 15, which can be clearly identified by the ECT system.

D. Discussions

The flow patterns of the two-phase flow are relative simple in the CCS chain, i.e. stratified and homogenous. In this case, when the three algorithms in this paper are used to calculate the gas holdup, the absolute errors have no obvious difference. Compared with the LBP and Calderon algorithms, the Landweber algorithm can provide lower standard deviation in an iterative way. However, the parameter selection is crucial and the computing time is long if more iteration times are required in the Landweber algorithm. The single-step algorithms, i.e. the LBP and Calderon algorithms, can significantly shorten the computing time. Compared with the LBP algorithm, the Calderon algorithm is more applicative for complex flow patterns [25]. In consideration of the requirements of real-time and applicability, the Calderon algorithm is suggested in this paper.

The reconstruction method used in this paper is based on a 2D model. In the future, a 3D reconstruction method can be used to provide axial resolution along the pipe. However, it may affect the real-time performance of the system.

V. CONCLUSIONS

This paper presented the potential of ECT for monitoring of carbon dioxide transport in pipelines. Experimental results have shown that

1) The stratified and homogeneous flow patterns of the two-phase CO_2 flow can be identified using the proposed method, which matches well with the images captured by the high-speed imaging system. The dynamic process of the CO_2 two-phase flow can be captured by the proposed ECT system with a high time resolution.
2) When the liquid flowrate rate is low, the flow pattern of the CO_2 flow is a stratified flow and the absolute errors and standard deviations of gas holdup measurements are relatively high. When the liquid flowrate rate is higher, the gaseous CO_2 and liquid CO_2 are mixed more evenly and the standard deviation is lower.
3) The maximum absolute errors of gas holdup measurements are 6.0% at the lower liquid flowrate, 3.2% at the medium liquid flowrate and 1.6% at the higher liquid flowrate, respectively, when using the Calderon algorithm.

REFERENCES

[1] S. Mirzaei, A. Shamiri, and M. K. Aroua, "A review of different solvents, mass transfer, and hydrodynamics for postcombustion CO2 capture," *Rev. Chem. Eng.*, vol. 31, no. 6, pp. 521–561, 2015.

[2] J. Gibbins and H. Chalmers, "Carbon capture and storage," *Energy Policy*, vol. 36, no. 12, pp. 4317–4322, Dec. 2008.

[3] H. Yang, Y. Qin, G. Feng, and H. Ci, "Online Monitoring of Geological CO2 Storage and Leakage Based on Wireless Sensor Networks," *IEEE Sens. J.*, vol. 13, no. 2, pp. 556–562, Feb. 2013.

[4] X. Cui, Y. Yan, Y. Ma, L. Ma, and X. Han, "Localization of CO2 leakage from transportation pipelines through low frequency acoustic emission detection," *Sens. Actuators Phys.*, vol. 237, pp. 107–118, Jan. 2016.

[5] K. Adefila, Y. Yan, L. Sun, and T. Wang, "Flow measurement of wet CO2 using an averaging pitot tube and coriolis mass flowmeters," *Int. J. Greenh. Gas Control*, vol. 63, pp. 289–295, Aug. 2017.

[6] T. Green, M. Reese, and M. Henry, "Two-Phase Co2 Measurement and Control in the Yates Oil Field," *Meas. Control*, vol. 41, no. 7, pp. 205–207, Sep. 2008.

[7] L. Wang, Y. Yan, X. Wang, T. Wang, Q. Duan, and W. Zhang, "Mass flow measurement of gas-liquid two-phase CO 2 in CCS transportation pipelines using Coriolis flowmeters," *Int. J. Greenh. Gas Control*, vol. 68, pp. 269–275, Jan. 2018.

[8] X. Dong, C. Tan, and F. Dong, "Gas-Liquid Two-Phase Flow Velocity Measurement With Continuous Wave Ultrasonic Doppler and Conductance Sensor," *IEEE Trans. Instrum. Meas.*, vol. 66, no. 11, pp. 3064–3076, Nov. 2017.

[9] S. Ren, H. Liu, C. Tan, and F. Dong, "Tomographic Wire-Mesh Imaging of Water-Air Flow Based on Sparse Minimization," *IEEE Sens. J.*, vol. 17, no. 24, pp. 8187–8195, Dec. 2017.

[10] Z. Cao and L. Xu, "Direct recovery of the electrical admittivities in 2D electrical tomography by using Calderon's method and two-terminal/electrode excitation strategies," *Meas. Sci. Technol.*, vol. 24, no. 7, p. 074007, Jul. 2013.

[11] Y. Yan and N. Jin, "Measurement techniques for multiphase flows," *Flow Meas. Instrum.*, vol. 27, p. 1, Oct. 2012.

[12] D. L. George, J. R. Torczynski, K. A. Shollenberger, T. J. O'Hern, and S. L. Ceccio, "Validation of electrical-impedance tomography for measurements of material distribution in two-phase flows," *Int. J. Multiph. Flow*, vol. 26, no. 4, pp. 549–581, Apr. 2000.

[13] C. Rautenbach, M. C. Melaaen, and B. M. Halvorsen, "Statistical diagnosis of a gas-solid fluidized bed using Electrical Capacitance Tomography," *Int. J. Multiph. Flow*, vol. 49, pp. 70–77, Mar. 2013.

[14] R. Banasiak *et al.*, "Study on two-phase flow regime visualization and identification using 3D electrical capacitance tomography and fuzzy-logic classification," *Int. J. Multiph. Flow*, vol. 58, pp. 1–14, Jan. 2014.

[15] S. Sun, Z. Cao, A. Huang, L. Xu, and W. Yang, "A High-Speed Digital Electrical Capacitance Tomography System Combining Digital

Recursive Demodulation and Parallel Capacitance Measurement," *IEEE Sens. J.*, vol. 17, no. 20, pp. 6690–6698, Oct. 2017.
[16] I. Ismail, J. C. Gamio, S. F. A. Bukhari, and W. Q. Yang, "Tomography for multi-phase flow measurement in the oil industry," *Flow Meas. Instrum.*, vol. 16, no. 2, pp. 145–155, Apr. 2005.
[17] W. Warsito and L.-S. Fan, "Measurement of real-time flow structures in gas–liquid and gas–liquid–solid flow systems using electrical capacitance tomography (ECT)," *Chem. Eng. Sci.*, vol. 56, no. 21, pp. 6455–6462, Nov. 2001.
[18] Z. Cui *et al.*, "A review on image reconstruction algorithms for electrical capacitance/resistance tomography," *Sens. Rev.*, vol. 36, no. 4, pp. 429–445, 2016.
[19] L. Xu, S. Sun, Z. Cao, and W. Yang, "Performance analysis of a digital capacitance measuring circuit," *Rev. Sci. Instrum.*, vol. 86, no. 5, p. 054703, May 2015.
[20] A. D. Okonkwo, M. Wang, and B. Azzopardi, "Characterisation of a high concentration ionic bubble column using electrical resistance tomography," *Flow Meas. Instrum.*, vol. 31, no. Supplement C, pp. 69–76, Jun. 2013.
[21] W. Tian, J. Sun, M. F. Ramli, J. Wang, and W. Yang, "An Electrical Capacitance Tomography Sensor With Variable Diameter," *Ieee Sens. J.*, vol. 17, no. 7, pp. 2089–2099, Apr. 2017.
[22] W. Q. Yang and L. H. Peng, "Image reconstruction algorithms for electrical capacitance tomography," *Meas. Sci. Technol.*, vol. 14, no. 1, pp. R1–R13, Jan. 2003.
[23] W. Q. Yang, D. M. Spink, T. A. York, and H. McCann, "An image-reconstruction algorithm based on Landweber's iteration method for electrical-capacitance tomography," *Meas. Sci. Technol.*, vol. 10, no. 11, p. 1065, 1999.
[24] W. Tian, J. Sun, M. F. Ramli, and W. Yang, "Adaptive Selection of Relaxation Factor in Landweber Iterative Algorithm," *IEEE Sens. J.*, vol. 17, no. 21, pp. 7029–7042, Nov. 2017.
[25] Z. Cao, L. Xu, W. Fan, and H. Wang, "Electrical Capacitance Tomography for Sensors of Square Cross Sections Using Calderon's Method," *IEEE Trans. Instrum. Meas.*, vol. 60, no. 3, pp. 900–907, Mar. 2011.

Shijie Sun (M'17) received the B.Sc. degree in automation from Tianjin University, Tianjin, China, in 2011 and received the Ph.D. degree in measurement technology and instruments from Beihang University, Beijing, China, in 2017. He is currently a post-doctor in Beihang University, Beijing, China. His current research interests include electrical tomography and digital signal processing.

Wenbiao Zhang (M'15) received the B.Eng. degree in automation, the M.Sc. and Ph.D. degrees in measurement technology and automatic devices from Tianjin University, Tianjin, China, in 2008, 2010, and 2014, respectively.He is currently a Lecturer with the School of Control and Computer Engineering, North China Electric Power University, Beijing, China. His research interests include multiphase flow measurement techniques and development of instrumentation systems

Jiangtao Sun (M'12) received the B.Eng. and M.Eng degree in measurement and control technology and instrument from Xidian University, Shaanxi, China, in 2008 and 2010, respectively, and the Ph.D. degree in electrical and electronic engineering from The University of Manchester, Manchester, U.K., in 2014. He is currently an associate professor in Instrumentation Science with Beihang University, Beijing, China. His research interests include electrical capacitance tomography and electrical impedance tomography for industrial and biomedical applications.

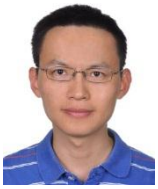

Zhang Cao (M'10) received the B.Sc. degree (with distinction) in automation and the M.Eng. and Ph.D. degrees (with distinctions) in measurement technology and automatic devices from Tianjin University, Tianjin, China, in 2003, 2005, and 2008, respectively. He is currently a professor with the School of Instrumentation Science and Opto-Electronic Engineering, Beihang University, Beijing, China. His interests include process tomography, multiphase flow measurement, and inverse problems.

Lijun Xu (M'04–SM'04) received the B.Sc., M.Eng., and Ph.D. degrees in electrical engineering and instrumentation from Tianjin University, Tianjin, China, in 1990, 1993, and 1996, respectively. From 1997 to 2001, he was an Associate Professor with the School of Electrical Engineering and Automation, Tianjin University.

From January 2002 to December 2004, he was a Research Fellow with the University of Greenwich at Medway, Chatham, U.K., and the University of Kent, Canterbury, U.K. From December 2004 to April 2006, he was a Higher Scientific Officer with the Department of Physics, Institute of Cancer Research, University of London, London, U.K. He is currently a Professor with the School of Instrument Science and Opto-Electronic Engineering, Beihang University, Beijing, China. He has authored or coauthored more than 260 publications. His current research interests include digital imaging and dynamic process monitoring. His current research interests include tomographic imaging, scanning imaging and dynamic process monitoring. He won the National Science Fund for Distinguished Young Scholars, the Ministry of Education Technology Invention Award (1st class) and China Instrument Society Science and Technology Award (1st class) in 2012, 2012 and 2014, respectively. He was elected as a Chang-Jiang Scholars Program Professor and a National High-Level Personnel of Special Support Program by the Ministry of Education, Ministry of Organisation, China, in 2014 and 2016, respectively.

Yong Yan (M'04–SM'04–F'11) received the B.Eng. and M.Sc. degrees in instrumentation and control engineering from Tsinghua University, Beijing, China, in 1985 and 1988, respectively, and the Ph.D. degree in flow measurement and instrumentation from the University of Teesside, Middlesbrough, U.K., in 1992.

He was an Assistant Lecturer with Tsinghua University in 1988. He joined the University of Teesside in 1989, as a Research Assistant. After a short period of post-doctoral research, he was a Lecturer with the University of Teesside from 1993 to 1996, and then as a Senior Lecturer, Reader, and Professor with the University of Greenwich, Chatham, U.K., from 1996 to 2004. He is currently a Professor of Electronic Instrumentation, the Head of the Instrumentation, Control and Embedded Systems Research Group, and the Director of Research with the School of Engineering and Digital Arts, University of Kent, Canterbury, U.K. He has been a 1000-Talent-Plan Scholar at North China Electric Power University, Beijing, China since 2011.